Unveiling the degradation mechanism of cathodic MoS2/C electrocatalysts for PEMWE applications

Keyla Teixeira Santos, Luz Adela Zavala Sanchez, Vincent Martin, François Guillet, Kavita Kumar, Xavier Portier, Frédéric Maillard, Laetitia Oliviero, Laetitia Dubau

Unveiling the degradation mechanism of cathodic MoS_2/C electrocatalysts for PEMWE applications

Keyla Teixeira Santos[a], Luz Adela Zavala Sanchez[b], Vincent Martin[a], François Guillet[a], Kavita Kumar[a], Xavier Portier[c], Frédéric Maillard[a], Laetitia Oliviero[b,*], Laetitia Dubau[a,*]

a. Univ. Grenoble Alpes, CNRS, Grenoble INP, Univ. Savoie Mont Blanc, LEPMI, 38000 Grenoble, France

b. Laboratoire Catalyse et Spectrochimie, Normandie Université, ENSICAEN, UNICAEN, 6, bd du Maréchal Juin, 14050 Caen, France

c. Centre de Recherche sur les Ions, les Matériaux et la Photonique, Normandie Université, ENSICAEN, UNICAEN, CNRS, 6, bd du Maréchal Juin, 14050 Caen, France

* Corresponding authors.

E-mail address: laetitia.dubau@grenoble-inp.fr, laetitia.oliviero@ensicaen.fr

KEYWORDS

Proton Exchange Membrane Water Electrolyzer (PEMWE), Non-noble electrocatalyst, Hydrogen Evolution Reaction (HER), Molybdenum Sulfides, Durability in realistic conditions, online ICP-MS.

ABSTRACT

Molybdenum dichalcogenides (MoS_2) are promising non-noble alternatives to replace platinum (Pt) for Hydrogen Evolution Reaction (HER) electrocatalysis in Proton Exchange Membrane Water Electrolyzers (PEMWE). The knowledge acquired on this class of catalyst for hydrodesulfurization (HDS) reactions has enabled significant advances in designing active MoS_2 for HER. However, the stability of MoS_2 in the dynamic operating conditions of a PEMWE coupled to renewable energy sources is often overlooked in the literature and is the focus of the present work. Herein, using nano slabs of 2H MoS_2 supported on high surface area carbon, we dynamically monitored Mo dissolution trends both under HER conditions and at more anodic potentials to mimic start-ups and shut-downs of a PEMWE device. We report minimal Mo dissolution under

HER conditions but it continuously increased with higher electrode potentials. In particular, Mo dissolution peaked during the irreversible oxidation from Mo(IV) to Mo(VI) starting at E = 0.7 V_{RHE} which in turn fully annihilates HER activity. Since no change in Mo and S surface composition was observed, the decline in HER activity was attributed to the continuous exfoliation of the 2D MoS_2 stacked layers induced by oxidation/dissolution of Mo. Additionally, our findings indicate that Mo cations can redeposit onto the cathode catalytic layer, forming a Mo blue film primarily composed of Mo(VI) species. This redeposition hampers HER performance by blocking catalytic sites and diminishing the catalyst's overall efficiency. These insights demonstrate the need to avoid excursions above E = 0.6 V_{RHE} for the safe use of MoS_2 cathode catalyst in PEMWE.

1. Introduction

Hydrogen, hailed as the "fuel of the future," stands at the forefront of the global energy transition, poised to revolutionize the way we produce, store, and utilize energy. As the world strives for decarbonization and sustainability, hydrogen emerges as a versatile and clean energy carrier with the potential to address pressing environmental challenges and reshape the energy landscape [1,2]. In the quest for sustainable energy solutions, the widespread adoption of renewable hydrogen production technologies, such as proton exchange membrane water electrolyzers (PEMWEs) is crucial [3]. Despite their reliability, the large-scale deployment of PEMWEs is hindered by the scarcity and consequent high cost of platinum group metals (PGMs), which are utilized as catalysts for both the oxygen evolution reaction (OER) and the hydrogen evolution reaction (HER). This challenge has spurred intensive research efforts into the development of alternative HER catalysts based on earth-abundant non-noble metals, aiming to reduce the reliance on PGMs in PEMWEs [4,5].

Among various non-PGM catalysts for the HER, nanostructured molybdenum disulfide (MoS_2) stands out as one of the most promising candidates [6–11]. It has been theoretically and experimentally demonstrated that the active sites are located at its edges, while the basal planes remain inactive for HER [10,12]. Considerable efforts have been devoted to improving HER kinetics to approach the performance of carbon-supported platinum nanoparticles (Pt/C) [11]. This promising HER activity has enabled MoS_2 to be

implemented in PEMWE cathodes, paving the way for more cost-effective and sustainable hydrogen production [13,14]. Studies on catalyst composition and morphology indicate that the crystalline phases of MoS_2 critically influence its activity in the HER [15,16]. MoS_2 can adopt various structures, including the semiconducting 2H phase [17], the metallic 1T phase [18], and the less common 3R phase [19]. Each phase exhibits distinct Mo-S atomic arrangements and stacking configurations across a long-range periodic structure. Thermodynamically, the 2H phase is the most stable, and despite its semiconducting character, it appears to be the best long-term strategy. The 1T phase has been reported to evolve into the 2H phase upon HER operating conditions [20].

Although the wide comprehensive approach towards the composition and catalyst activity, the stability of this class of material remains poorly investigated, particularly in conditions of power shutdowns or simple on-off of the PEMWE in a context of intermittent power input, characteristic of renewable energy sources as photovoltaic or wind energy [21]. Among the few studies examining MoS_2 stability under non-HER potentials, Ledendecker et al [22] combined operational protocols with *in situ* approaches to unveil the degradation phenomena across various material classes in acidic electrolyte, including MoS_2. They found that the catalyst exhibited high stability during the HER, even under harsh potential cycling conditions. However, significant corrosion occurred at open-circuit potential (OCP), a behavior also observed in other non-precious HER catalysts [23,24]. In another study, Wang et al [25] also evidenced the MoS_2's robustness under acidic HER conditions using a computed Pourbaix diagram to analyze the stability of four well-known active non-precious HER catalysts under working conditions, identifying the origin of the instability at OCP as stemming from the large thermodynamic decomposition driving force at high potential then at cathodic operation. The stability of these catalysts was verified by measuring the Mo dissolution rate using Inductively-Coupled Plasma Mass Spectrometry (ICP-MS). The calculated diagram predicted MoS_2 to be stable up to 0.35 V_{RHE}, which was inconsistent with the experimental results showing higher Mo dissolution at 0.23 V_{RHE} than under HER conditions. This discrepancy remains unexplained. Recently, Escalera-López et al. [26] provided valuable insights into the stability of lamellar-like MoS_2 and cluster-like amorphous MoS_{3-x} during HER operation. Using ICP-MS coupled with a scanning flow cell (SFC-ICP-MS) to monitor the Mo and S dissolution profiles, they found that the stability of MoS_2 depends on the nature of its allotrope. Furthermore, they demonstrated that Mo dissolution is more significant during 0 V_{RHE} holds than at HER potentials.

Coupling renewable energy sources with electrolyzers provides an ideal strategy for achieving hydrogen production as a clean fuel [27]. However, it raises a severe stability issue as, when integrated with renewable energy sources like solar or wind, a PEMWE device experiences seasonal power fluctuations, intentional or unintentional power shutdowns, or routine on-off cycles. In these conditions, the hydrogen and oxygen present in the stack are chemically consumed and a rise in cathode voltage is observed, which can degrade the catalyst and reduce the electrochemically active surface area, impacting the system's efficiency [28,29]. Unlike platinum, which remains stable barring transient oxide formation/reduction, the durability of earth-abundant materials is likely to be compromised under these intermittent power conditions [30]. Moreover, if the cathode catalyst dissolves, the produced metal cations are likely to ion exchange within the sulfonic acid end groups of the ionomer and/or membrane, leading to reduced ionomer conductivity, membrane degradation, dehydration, and consequently lower membrane conductivity [31].

Studies on the stability of non-noble HER catalysts remain underexplored and not fully understood, hindering their full potential in practical applications such as PEMWEs. Therefore, investigating the stability of MoS_2 catalysts under realistic operating conditions is imperative to ensure their reliability and durability in practical PEMWE devices. In this study, we dynamically monitored the dissolution behavior of MoS_2/C catalysts under different conditions using an online electrochemical flow cell coupled with an ICP-MS (FC-ICP-MS). Our comprehensive approach combines real-time monitoring and post-experimental analysis to provide a detailed understanding of the changes of MoS_2/C catalyst under HER conditions as well as at more anodic ($E > 0\ V_{RHE}$) potentials, mimicking fluctuating renewable energy input that PEMWE devices experience. Further, we simulate conditions with a high concentration of dissolved Mo species to investigate the potential impact of excess of Mo dissolved species on catalyst performance. These insights can contribute to establishing of guidelines for the safe use of MoS_2 for HER in PEMWE devices.

2. Experimental Section

2.1. Catalyst Synthesis

The MoS_2 catalyst used in this study was prepared by an aqueous impregnation solutions method, as previously reported [32,33]. Pre-defined amounts of ammonium heptamolybdatetetrahydrate ($(NH_4)_6Mo_7O_{24}\cdot 4H_2O$, Merck) and citric acid (CA) ($C_6H_8O_7\cdot H_2O$, Prolabo), both without further purification, were dissolved in Ultrapure MilliQ (Millipore, 18.2 MΩ cm, total organic compounds < 3 ppb) water at ambient temperature to obtain a CA/Mo = 2 and the pH adjusted to 0.01. The solution was impregnated on a carbon black support (Vulcan XC 72 Cabot Corp.) by stirring for 2h. To obtain the catalyst in its sulfide form, a sulfidation procedure was performed at 350 °C at a heating rate of 3 °C min^{-1} at 0.1 MPa for 2 h under a 30 cm^3 min^{-1} flow of 10% H_2S/H_2. The catalytic suspension was prepared by mixing the catalyst powder, a diluted Nafion solution (5 wt % in a mixture of lower aliphatic alcohols and water), isopropanol, and ultrapure water (Millipore, 18.2 MΩ cm, total organic compounds < 3 ppb). The catalytic ink was homogeneously dispersed in an ultrasonic bath for 20 min.

2.2. TEM and High-Resolution Scanning Transmission Electron Microscopy—High Angular Annular Dark Field (HRSTEM-HAADF)

The slab nanostructure and morphology of the catalyst were determined by high resolution transmission microscopy (HR TEM) and scanning transmission electron microscopy (HR STEM) with a high angle annular dark field (HAADF) detector. Images were obtained with a double corrected JEOL ARM 200F cold FEG microscope operated at 200 kV. The sulfide catalyst was deposited on a 300-mesh copper grid with holey carbon film. The images were treated by the commercial software GMS3 from GATAN (DIGITALMICROGRAPH) and free Mesurim software. The acquisition of one image lasted about 30 s with a resolution of 1024 pixels × 1024 pixels, (30 μs of exposure time for each spot in the scanning mode).

2.3. Electrochemical Measurements

The HER activity measurements were conducted in a four-electrode electrochemical cell thermostated at T = 25 °C. The Load Cycle (LC) measurements were performed using a two-compartment H-cell. In both cases, a glassy carbon rotating disk (area = 0.196 cm^2) was used as substrate for depositing a thin-layer film of catalyst, which served as working

electrode. A polished glassy carbon plate and a daily-prepared reversible hydrogen electrode (RHE) were used as counter and reference electrodes, respectively. Additionally, a platinum wire was connected in series with the RHE to filter the electronic noise. The working electrode was placed in the right compartment of the H-cell along with the reference electrode and the Pt wire. Separated by a glass frit, the left compartment contained the counter electrode. Before use, all glassware was cleaned in a 1:1 H_2SO_4: H_2O_2 solution for at least 12 h, then carefully rinsed and boiled with ultrapure water (Millipore, 18.2 MΩ cm, total organic compounds < 3 ppb). Prior to the experiments, the 0.5 M H_2SO_4 electrolyte solution (H_2SO_4 Suprapur 96%, Merck) was de-aerated with argon (Ar > 99.999 %, Messer). The electrochemical experiments were performed using an Autolab PGSTAT 302N potentiostat. The potential was maintained at E = 0.05 V *vs*. RHE) to insert the working electrode in the cell. All electrode potentials are referred to the RHE. Prior to each LC, 20 cyclic voltammograms (CVs) were conducted, weeping the electrochemical potential from 0.1 to -0.3 V_{RHE} at a scan rate of 10 mV s^{-1} in an Ar-purged 0.5 M H_2SO_4 electrolyte with the electrode rotating at 1600 rpm. The overpotential at a current density of 10 mA cm^{-2}_{geo} (η_{10}) was used as the metric to evaluate the catalyst's activity before and after the LCs. All electrochemical measurements included dynamic iR-correction, with solution resistance assessed through electrochemical impedance spectroscopy.

2.4. Inductively-Coupled Plasma Spectrometer (ICP-MS) coupled to an Electrochemical Flow cell (FC-ICP-MS)

The electrolyte from the working electrode compartment was analyzed with ICP-MS to quantify the amount of Mo dissolved during the LC experiments. Before analyses, the ICP-MS instrument (NexION 2000c, PerkinElmer, Inc., Waltham, Massachusetts, USA) was optimized for maximum elemental sensitivity. Five-point calibration curves were obtained with freshly prepared calibration solutions of ^{98}Mo at concentrations of 0, 5, 10, 20, and 50 µg L^{-1}. These solutions were prepared from single-element ICP-MS standard solutions (Carl Roth GmbH & Co. KG, Germany) and diluted in 0.05 M H_2SO_4 (Carl Roth Rotipuran® Ultra, 70% H_2SO_4 in ultrapure water – MilliQ, 18.2 MΩ cm, TOC < 3 ppb).

The stability of the MoS_2/C samples was also evaluated *in situ*, using an online FC-ICP-MS setup, as detailed in Ref. [33]. Calibration profiles showed no significant differences

whether the electrolyte bypassed or flowed through the electrochemical flow cell. For the FC-ICP-MS measurements, an Autolab potentiostat (PGSTAT302N) was used in a three-electrode configuration. The electrochemical flow cell comprised a single compartment made of Teflon® and housed a three-electrode system. The working electrode was a glassy carbon disk (5 mm diameter) embedded in Teflon, the counter electrode was a glassy carbon rod (Sigradur®, HTW), and the reference electrode was a commercial miniature Ag/AgCl/3.4 M Cl^- electrode (ET072, eDAQ). Thin-film of MoS_2/C were deposited on the working electrode by drop-casting 10 µL of an ultrasonically homogenized catalyst suspension, resulting in a loading of approximately 40 µg Mo cm^{-2}_{geo}. The electrolyte, 0.05 M H_2SO_4 (Rotipuran Ultra, Carl Roth), was freshly prepared, de-aerated with Ar (99.999%, Messer), and continuously pumped from a reservoir through the electrochemical flow cell using the ICP-MS peristaltic pump at a flow rate of 430 µL min^{-1}. Each FC-ICP-MS measurement was repeated at least twice using independent thin-film electrodes, with error bars representing the standard deviation of these measurements. All experiments were conducted at 22 ± 2 °C, and all potentials are reported relative to the reversible hydrogen electrode (RHE).

2.5. X-ray photoelectron spectroscopy (XPS)

Before and after LC measurements, XPS analyses were conducted on the catalyst film using a Thermo Scientific™ *K*-Alpha spectrometer equipped with a monochromatized Al *K*α X-ray source (hν = 1486.6 eV) and a spot size of 400 µm. Core level spectra were recorded using a pass energy of 30 eV, while survey spectra were acquired at a pass energy of 100 eV. To mitigate any positive charge accumulation on the sample surface during spectra acquisition, an electron flood gun was employed. The Mo 3d and S 2p regions of the XPS spectra were processed using CasaXPS (version 2.3.25PR1.0) software. Mo 3d and S 2p spectra were fitted by applying a 3/2 and 2/1 area ratio constraints on the $3d_{5/2:3/2}$ and $2p_{3/2:1/2}$ spin-orbit doublets, respectively.

3. Results and Discussion

3.1 Monitoring MoS_2/C dissolution in HER conditions by FC-ICP-MS

2H MoS_2 polymorph supported on high surface area carbon was synthesized according to our previous work [33,34]. The addition of citric acid was used to tune the size and stacking capability of the MoS_2 slabs, thereby optimizing the density of HER active edge sites [32,35]. **Figure 1a** and **b** show typical low magnification TEM images. Despite the poor contrast between MoS_2 and the carbon support, the crystallinity on MoS_2 allows to distinguish the MoS_2 slabs surrounding the surface of the carbon aggregates. The number of stacked layers is comprised between 2 and 5. **Figure 1c** presents atomically resolved HR-STEM-HAADF image of MoS_2/C highlighting the catalyst's morphology. The image demonstrates the successful synthesis on nanoslabs with an averaged particle size centered around 1.4 nm [35].

Figure 1d shows the HER polarization curves obtained before and after the break-in protocol, which consisted of 20 CVs ranging from 0.1 to -0.25 V_{RHE}. The initial polarization curve features a broad reduction peak at -0.05 V_{RHE}, attributed to the conversion of MoS_3 to MoS_2 [36], and/or to the reduction of MoO_xS_y (partially sulfided or oxysulfide) species [37]. Following the break-in procedure, the overall HER activity was maintained, indicating that the catalyst preserved its performance post-activation in agreement with previous reports [26].

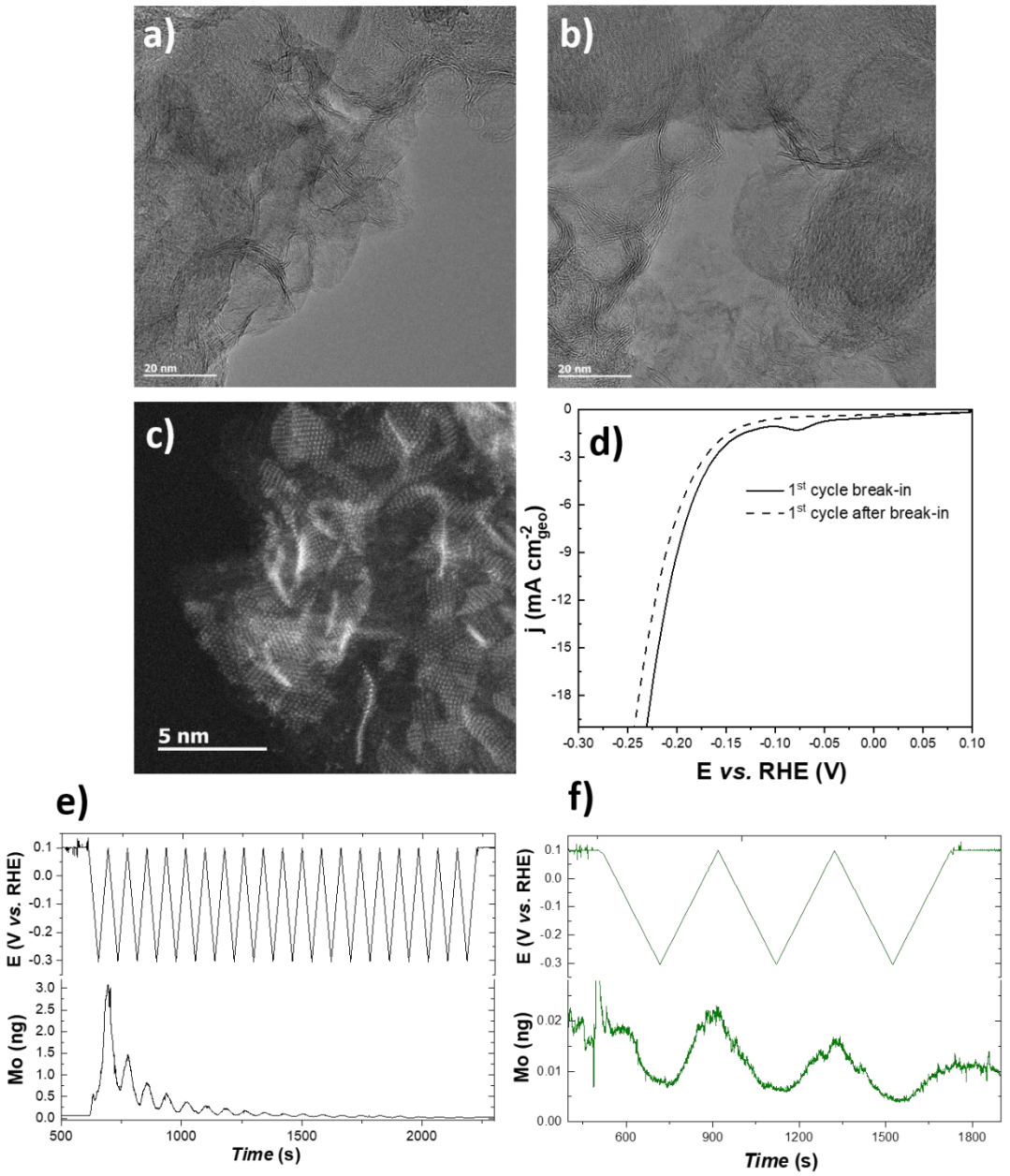

Figure 1. a) and **b)** Representative TEM images of MoS_2/C **c)** STEM-HAADF micrographs of 2H-MoS_2/C. **d)** HER polarization curves measured before and after the break-in protocol. Online FC-ICP-MS measurements obtained during **e)** the break-in protocol consisting of 20 CVs from 0.1 to -0.3V_{RHE} at 10 mV s^{-1}, **f)** 3 CVs from 0.1 to -0.3 V_{RHE} at 2 mV s^{-1}.

To quantitatively rationalize the decrease in HER activity during the break-in protocol, we conducted *in situ* monitoring of Mo dissolution during sequential CVs. The electrochemical break-in protocol and its associated dissolution profile were recorded over successive CVs within the HER potential window, as depicted in **Figure 1e**.

Significant Mo dissolution occurred in the first CV cycles stabilizing towards a steady state in the final 10 cycles of the activation protocol. This behavior is likely due to oxysulfides formed during incomplete sulfidation in the synthesis process, which are unstable and prone to rapid dissolution in acidic electrolyte [37].

Figure 1f illustrates the Mo dissolution behavior at a slow scan rate of 2 mV s^{-1} within the HER potential window (0.1 to -0.3 V_{RHE}). This slower potential scan rate enhances FC-ICP-MS resolution and provides detailed insights into the dissolution dynamics under HER conditions. The Mo dissolution signal remains similar at 2 and 10 mV s^{-1}, albeit with lower intensity during the slower CV cycles, confirming the predominance of the stable MoS_2 phase. According to the calculated Pourbaix diagram [25], MoS_2 is predicted to be stable around 0 V_{RHE}, hence, the increase in the Mo dissolution rate during the anodic sweep up to 0.1 V_{RHE} can be attributed to the undercoordinated Mo species produced under HER potentials which are destabilized at non-cathodic potentials and prompt to dissolve [26].

3.2 Monitoring MoS_2/C dissolution in anodic conditions and impact on HER activity

As mentioned in the introduction, the cathode catalytic layer is prone to experience excursions at high anodic potential, especially during stop events such as those encountered in PEMWE systems coupled with intermittent renewable energy sources [30]. The cathodic potential can reach 0.8-0.9 V_{RHE} under atmospheric H_2 production conditions, and this is particularly true without circulation of water during the stop events [38]. Therefore, investigating how the extent of MoS_2 oxidation impacts the HER activity and the degree of Mo dissolution is crucial for practical use of MoS_2 in industrial PEMWE devices.

To gain quantitative insights into the changes in HER activity, we first conducted CVs with various upper potential limit (UPL) to 0.6, 0.8, 1.05, and 1.23 V_{RHE} in a conventional three-electrode glass cell with 0.5 M H_2SO_4 as the electrolyte, as depicted in **Figure 2a-d**. The lower potential limit (LPL) was kept constant at -0.3 V_{RHE} to evaluate the impact of MoS_2 oxidation on HER activity. While a positive potential excursion at 0.6 V_{RHE} shows no significant changes, a slight increase in the anodic current began to be observed at a UPL of 0.8 V_{RHE}, which became progressively more pronounced with higher UPLs. A distinct oxidation peak appeared at approximately 0.7 V_{RHE}, becoming fully resolved

when the UPL reached 1.23 V_{RHE} (note that it is highly unlikely for a PEMWE cathode to reach this potential; it is used to better illustrate the Mo dissolution trend). This peak corresponds to the irreversible oxidation of Mo(IV) to Mo(VI) and is accompanied by a pronounced decrease in HER activity, signing the deactivation of the HER active sites. To better mimic PEMWE operating conditions, the influence of the temperature was studied with measurements conducted at 40, 60 and 80 °C (Figure S1). The results indicate faster HER kinetics and show that the MoS_2 oxidation peak shifts negatively when the temperature increases. Specifically, irreversible MoS_2 oxidation occurs between 150 and 200 mV earlier at 80°C compared to ambient temperature confirming the significant role temperature plays in the deactivation of MoS_2/C catalysts, and suggesting that the cathode potential should not exceed 0.6 V_{RHE} in a real PEMWE device operating at 80°C.

According to the irreversible oxidation reaction of MoS_2 described by [39]:

$$MoS_2 + 3H_2O \rightarrow MoO_3 + S_2^{2-} + 6H^+ + 4e^- \quad (1)$$

In that scenario, the electrical charge under the oxidation peak corresponds to the complete oxidation of MoS_2 initially loaded on the electrode, as per the Faraday law. It is however important to note that we have considered an extreme case and that other oxidative reactions involving more electrons are possible. As a result, substantial oxidation of MoS_2 coincides with the Mo dissolution trends observed in the FC-ICP-MS measurements. **Figure 2e and f** display Mo dissolution signal over a broader potential range from -0.3 V to 0.8 V_{RHE}, and 1.23 V_{RHE}, respectively. At this potential, the catalyst is promptly decomposed in MoO_3 and HSO_4^-. According to the calculated Pourbaix diagram from Ref. [25], the oxidation of Mo(IV) into MoO_3 begins at E = 0.7 V_{RHE}, consistent with the presence of a shoulder on the Mo dissolution signal shown in **Figure 2e**. Extending the potential range to a higher UPL of 1.23 V_{RHE} (**Figure 2f**) marks maximal Mo dissolution during the first cycle, as no Mo dissolution is measured for the second and third potential sweeps. Furthermore, both the Mo dissolution profile and current reach their maximum at *ca.* 1 V_{RHE}.

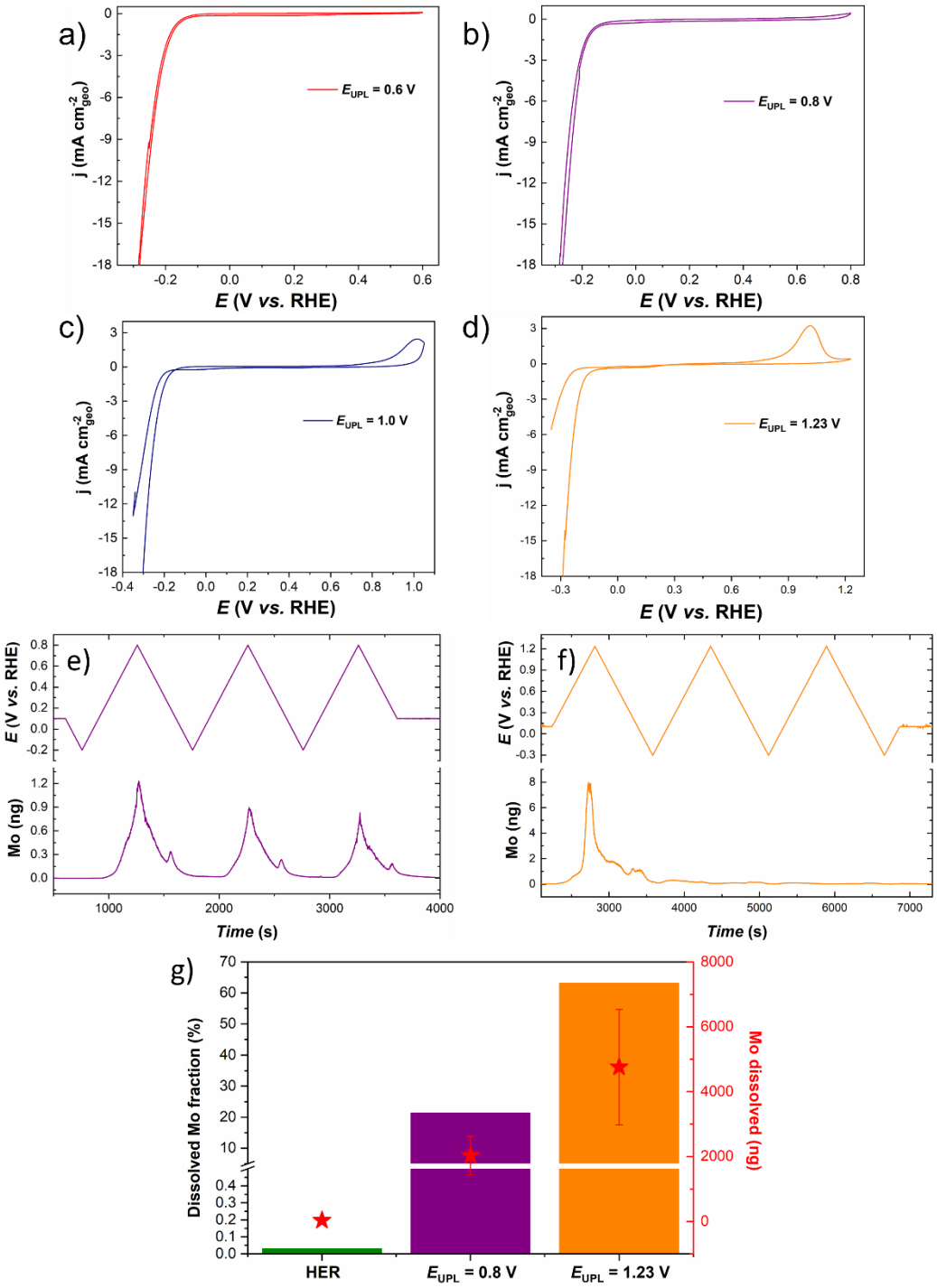

Figure 2. Cyclic voltammograms recorded on MoS_2/C in 0.5M H_2SO_4 at a scan rate of 2 mV s^{-1} scanning from -0.35 V to **a)** 0.6 V; **b)** 0.8 V; **c)** 1.05 V and **d)** 1.23V. Online FC-ICP-MS obtained for **e)** 3 CVs from -0.20 to 0.8V or from **f)** -0.3 to 1.23 V at 2 mV s^{-1} **g)** Graphical representation of the calculated amount of Mo dissolved under HER conditions and at high UPL of 0.8 and 1.23V, all referenced to RHE.

Figure 2g compares the amount of dissolved Mo and the corresponding percentage with respect to the initially loaded Mo on the working electrode. The results indicate good

stability under HER conditions, with less than 0.5% of Mo dissolved. Significant Mo dissolution (*ca.* 20% of the total amount of Mo initially loaded onto the working electrode) occurs at E_{UPL} = 0.8 V_{RHE}, and the trend is magnified (*ca.* 70%) at E_{UPL} = 1.23 V_{RHE}, coinciding with the irreversible oxidation of MoS_2 into MoO_3. These results underscore the vulnerability of this class of catalyst to potential above 0.6 V_{RHE}.

3.3. MoS_2/C degradation mechanism during accelerated stress tests (AST) mimicking PEMWE start-up/shup-down events

The previous section provided crucial insights into potential limits that should be avoided to maintain the HER performance of MoS_2-based catalysts under realistic PEMWE conditions. Given that the analyses were conducted at a CV scale (short-time scale), it is interesting to subject the MoS_2/C catalyst to accelerated stress tests for a fine tuning of the UPL.

For this purpose, we designed AST protocols involving 500 square cycles of 3 seconds at -0.3 V_{RHE}, with various UPLs ranging from 0.1 V_{RHE} to 0.8 V_{RHE} (protocol LC1 to LC6 schematically represented in **Figure 3a**). In **Figure 3b**, the electrolyte analyzed by ICP-MS after these LCs indicates that the amount of dissolved Mo increases with the UPL. This trend is particularly pronounced for LC6, which has the highest UPL of 0.8V_{RHE}. This confirms that higher UPLs induce greater dissolution of Mo, likely due to MoO_3 formation at elevated potentials and its subsequent dissolution in acidic environment. As shown in the pink squares in **Figure 3b** and **Table S1**, the overpotential at 10 mA cm^{-2}_{geo} (η_{10}) remains similar to that of the freshly conditioned MoS_2/C catalyst. Moreover, the amount of Mo dissolved was also quantified after 1 hour at OCP (0.65 V_{RHE}) and also after three times longer AST, namely 1500 LC3, which reflect this stability up to high UPL (**Table S1)**. This finding suggests that the MoS_2/C catalyst's structural integrity and active sites are preserved when the potential does not exceed 0.6 V_{RHE}.

In contrast, noticeable degradation in HER performance was observed after LC5 and LC6 protocols, corresponding to E_{UPL} of 0.7 V_{RHE} and 0.8 V_{RHE}, respectively consistent with the onset potential of Mo oxidation/dissolution discussed in the previous section (**Figure 2)**. An increase in HER overpotential ($\Delta\eta_{10}$) (also in **Figure 3b**) of 133 and 818 mV associated with 56 and 84% of Mo dissolution, respectively, was reported after LC5 and

LC6 protocol respectively. These results can be attributed to the exfoliation of 2H-MoS_2 layers, which progressively reduces the density of edge active sites and HER activity [10,12].

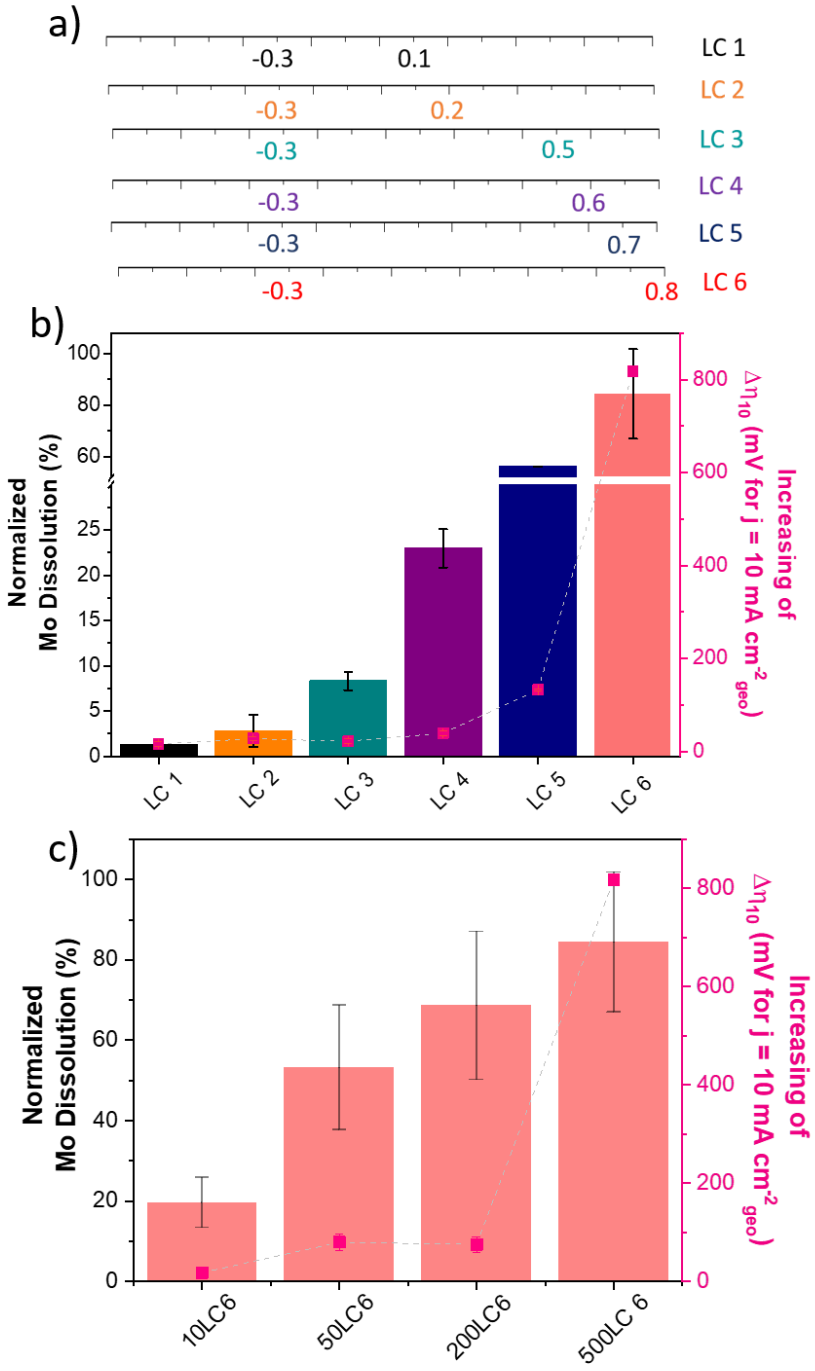

Figure 3. a) Schematic representation of the Load Cycle protocols involving variation of the upper potential limit from 0.1 to 0.8 V_{RHE} **b)** Normalized Mo dissolution for LC 1 to 6 protocols **c)** Normalized Mo dissolution for LC6 after 10, 50, 200 and 500 cycles. The right *y*-axis in a) and b) represents the increase in HER overpotential at

10 mA cm^{-2}_{geo} relative to the initial value after LCs. Error bars are the standard deviation of at least 3 independent measurements.

Figure 3c focuses on the LC 6 protocol (E_{UPL} = 0.8V_{RHE}) at intermediate ageing stages states (10, 50, 200 cycles). It is clear from this graph that the HER activity is null after 500 potential cycles. This result highlights that Mo dissolution progresses with cycle number, revealing time-dependent behavior. Interestingly, the impact of MoS_2/C oxidation on HER activity follows a different trend, showing minimal decline in HER performance until 200 cycles (despite 70% of Mo dissolved) but a significant drop thereafter. Hence, the notable Mo dissolution at higher UPLs combined with the mild impact of 200 potential cycles up to 0.8 V_{RHE} on HER activity, corroborates the hypothesis of continuous oxidation/dissolution of MoS_2 stacking sheets at high electrode potentials. The exfoliation of the MoS_2 layer occurs via MoO_x dissolution in acidic media, progressing over time at high potential. The MoS_2 layer being in contact with the carbon support should be more preserved by acidic chemical dissolution. The HER activity begins to decline when the layers and consequently the density of edge sites decreases significantly, indicating extensive Mo dissolution affecting the outer layers of MoS_2 in contact with the conductive carbon support, herein between 200 and 500 AST cycles. Interestingly after 500 AST cycles, ICP-MS measurements suggest no remaining Mo onto the electrode. Concurrently, the substantial increase in overpotential observed after 500 AST cycles (*ca*. 800 mV) can be attributed solely to HER activity on the carbon support [39]. Polarization curves before and after LCs protocols can be found in **Figure S2**.

To delve into the changes in chemistry after the various electrochemical conditions used in this study, XPS spectra were recorded after the initial CVs break-in and after 10, 50 and 200 LC6, as depicted in **Figure 4**.

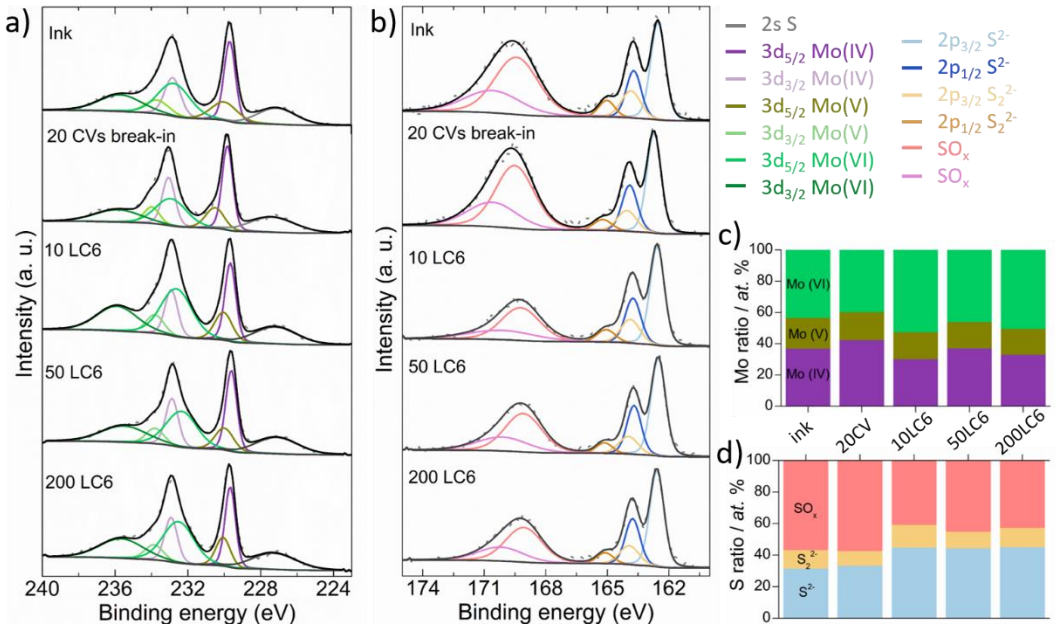

Figure 4. X-ray photoelectron spectra of MoS_2/C catalyst ink deposited on the glassy carbon electrode, after 20 CVs break-in protocol and after 10, 50 and 200 LC6 protocol of **a)** Mo 3d and **b)** S 2p. Relative atomic percentage distribution of **c)** Mo and **d)** S species.

As expected, following the initial break-in, the Mo (V) and Mo (VI) species diminish, while the Mo (IV) species becomes slightly more prominent, suggesting that the less stable Mo species have been removed, aligning with the FC-ICP-MS results during the break-in protocol (**Figure 1**). After 10, 50, and 200 LC6 cycles, **Figures 4a** reveals no significant differences in the Mo 3d spectra. This lack of variation suggests that the structure of the MoS_2 powder remaining onto the working electrode is similar to that of the initial state despite the AST. The absence of significant chemical changes in the Mo 3d spectra supports the hypothesis that exfoliation via Mo oxidation/dissolution is the main degradation mechanism at high potentials. The process of exfoliation exposes fresh MoS_2 sheets with similar surface chemistry then the fresh MoS_2/C catalyst, resulting in consistent XPS spectra despite extensive potential cycling and significant Mo dissolution. [36]. **Figure 4b** confirms this stability with the S 2p spectra. The S 2p peak positions and intensities show minor changes upon cycling (**Figure 4d**), suggesting that the sulfur environment, indicative of Mo-S bonding, remained largely unchanged even under the prolonged LC6 cycling conditions.

Last, we identified Mo redeposition as possibly detrimental to the HER activity (polyoxomolybdate cluster deposition may take place at the edge sites of MoS_2). Indeed, in technological PEMWE where the cathode may operate under steam or under water [40], the accumulation of Mo(V) and Mo (VI) ionic species produced from Mo dissolution could potentially deactivate the cathode catalyst. In solid electrolyte configuration, ionic species are more confined and thus more prone to be redeposited. Further, according to the Mo Pourbaix diagram, Mo cations can be reduced between E = -0.25 and E = -0.35 V_{RHE} in acidic conditions [41].

To mimic the confinement of Mo cations, we conducted CVs with an excess of Mo (VI) in liquid electrolyte and studied how they impact HER catalyst performance. Typically, 20 mM solution of ammonium heptamolybdate tetrahydrate in 0.5 M H_2SO_4 was used to simulate conditions with a high concentration of dissolved Mo (VI) species (**Figure 5a**). The rapid formation of a Molybdenum Blue (MB) film was observed as a result of the reduction of Mo (VI) species to mixed-valence polyoxomolybdate clusters in acidic conditions [42]. The presence of this film (inset in **Figure 5a**) could pose a significant issue in practical PEMWE systems, as it could block the HER active sites, and could lead to could lead to catalyst deactivation if not properly managed. This result highlights the importance of developing strategies to mitigate the Mo dissolution in practical PEMWE systems to maintain consistent HER activity. Mitigation strategies are generally classified into two categories: material strategies and system strategies. We believe it will be challenging to implement material strategies for MoS_2, as we showed that the decline in HER activity is attributed to the continuous exfoliation of the stacked 2D MoS_2 layers is caused by the oxidation and dissolution of Mo atoms at high electrode potentials. However, there are relevant system strategies in the PEMWE field. For instance, J. Parra et al. demonstrated that the cathode potential during the shutdown of a PEMWE device is influenced by whether the pump supplying water to the anode and cathode is operational. They observed that the cathode potential reaches 0.7 V_{RHE} when the water remains immobilized during the shutdown of the PEMWE, whereas it stays close to 0 V_{RHE} when water is circulated during the shutdown (see Figure 3.12 in ref [38]).

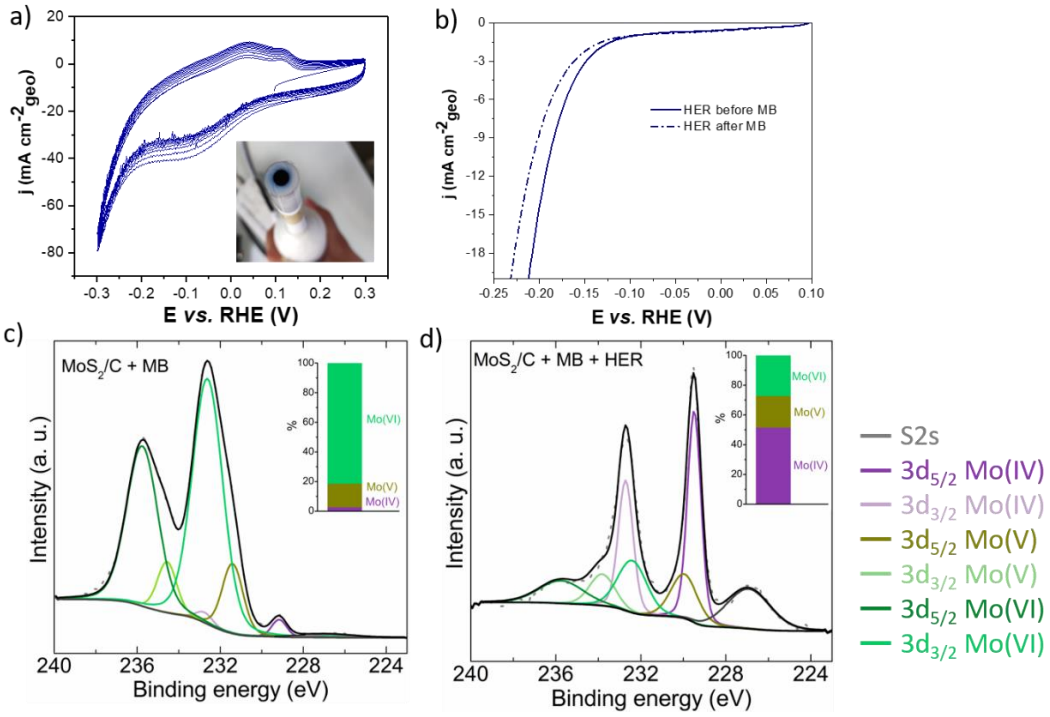

Figure 5. (a) Subsequent 10 cyclic voltammograms recorded from 0.3 to -0.3 V_{RHE} at 100 mV s^{-1} in a 20 mM solution of ammonium heptamolybdate tetrahydrate in 0.5 M H_2SO_4. Inset: Image of MB film formed on the MoS_2/C catalyst surface. **b)** Polarization curves before and after MB film reduction. Spectra of Mo 3d region of **c)** obtained from MoS_2/C catalysts after MB film formation and **d)** after the MB film was removed by replacing the electrolyte with 0.5 M H_2SO_4.

Importantly, the MB film was efficiently removed upon replacing the electrolyte with fresh 0.5 M H_2SO_4, and the MoS_2 surface was restored, with minimal impact on the HER activity (**Figure 5b**). The Mo 3d spectra of the MB film (**Figure 5c**) indicate a substantial presence of Mo (VI) on the electrode surface, nearly obscuring the underlying MoS_2. This suggests that the MB film covers the MoS_2 catalyst, significantly hindering its catalytic performance. After electrolyte replacement, although the catalyst surface appears fully restored (**Figure 5d**); a slight decrease in HER activity is shown in **Figure 5b**, where a 40 mV drop in η_{10} is observed after cycling the catalyst in a high concentrated Mo (VI) acid solution, indicating that some Mo from MoS_2 was leached along with the MB film.

4. Conclusion

MoS_2 electrocatalysts are among the most promising non noble and earth abundant candidates to replace Pt/C at the cathode of PEMWE devices. Although this catalyst exhibits high stability in HER conditions, caution has to be taken to avoid high cathode potentials encountered during PEMWE stop events. In this study, we investigated the degradation mechanisms of MoS_2/C by systematically varying the upper potential limit to simulate stop events of a PEMWE device. Online ICP-MS measurements indicate that irreversible oxidation of Mo occurs along with significant dissolution at $E \geq 0.6$ V_{RHE}, which adversely affects HER activity. Due to the semiconducting nature of MoS_2, not all edge active sites exhibit similar HER activity. Consequently, Mo dissolution and the loss of HER activity occur at different rates, with the active edge sites in contact with the carbon support being more preserved towards acidic chemical dissolution. This hypothesis is supported by XPS results showing that the chemical composition of the catalyst remaining on the electrode closely resembles that of the initial state. Furthermore, our results demonstrate that Mo cations can redeposit on the cathode's catalytic layer, forming a predominantly Mo (VI) species molybdenum blue film. This redeposition significantly impairs HER performance by obstructing active sites and reducing overall catalyst efficiency. Our result underscore the importance of carefully managing the stop event of PEMWE to prevent high potential excursions.

CRediT authorship contribution statement

Keyla Teixeira Santos: Investigation; Sample collection; Formal analysis; Drawing; Data curation; Writing – original draft. **Vincent Martin**: Sample collection and analysis; Investigation; Data curation. **Kavita Kumar:** Formal analysis; Drawing; Data curation. **François Guillet**: Sample collection and analysis; Data curation. **Luz Adela Zavala Sanchez**: Nanocatalysts synthesis, Sample collection and analysis. **Xavier Portier**: Sample collection and analysis. **Frédéric Maillard**: Methodology, Writing – review & editing. **Laetitia Oliviero**: Conceptualization; Funding acquisition; Resources; Project administration; Supervision; Methodology; Writing − review & editing. **Laetitia Dubau**: Conceptualization; Funding acquisition; Resources; Project administration; Supervision; Methodology, Writing − review & editing.

Declaration of competing interest

The authors declare the following financial interests/personal relationships which may be considered as potential competing interests:
Laetitia DUBAU reports financial support was provided by Carnot Energies du Futur. Laetitia OLIVIERO reports financial support was provided by Carnot ESP Institute. he other authors declare that they have no known competing financial interests or personal relationships that could have appeared to influence the work reported in this paper.

Appendix A. Supporting information

Supplementary data associated with this article can be found in the online version at DOI.

Funding Sources

The authors acknowledge the financial support of ANR CARNOT Energie et Systèmes de Propulsion (ESP) and ANR CARNOT Energies du Futur (EF) through the HERMOS project.

Acknowledgments

Laetitia Dubau: I would like to dedicate this work to our esteemed colleague, Prof. Elena Savinova of the University of Strasbourg, France. Her inspiring contributions have significantly advanced the field of electrocatalysis. On a personal note, when I think of Elena, I think of a dedicated and profoundly human scientist. She is always eager to share her vast experience and willing to learn, exchange ideas, and listen—whether as a jury member or over a glass of Valpolicella! Her enthusiasm shines just as brightly when discussing science as it does when recounting a chocolate cooking class she enjoyed with her grandchild. Many thanks, Elena, for the precious moments we've shared and for all the support you have given me.

5. References

[1] J.O.M. Bockris, The hydrogen economy: Its history, Int J Hydrogen Energy 38 (2013) 2579–2588. https://doi.org/10.1016/j.ijhydene.2012.12.026.

[2] Z. Abdin, A. Zafaranloo, A. Rafiee, W. Mérida, W. Lipiński, K.R. Khalilpour, Hydrogen as an energy vector, Renewable and Sustainable Energy Reviews 120 (2020) 109620. https://doi.org/10.1016/j.rser.2019.109620.

[3] M. Carmo, D.L. Fritz, J. Mergel, D. Stolten, A comprehensive review on PEM water electrolysis, Int J Hydrogen Energy 38 (2013) 4901–4934. https://doi.org/10.1016/j.ijhydene.2013.01.151.

[4] C. Van Pham, D. Escalera-López, K. Mayrhofer, S. Cherevko, S. Thiele, Essentials of High Performance Water Electrolyzers – From Catalyst Layer Materials to Electrode Engineering, Adv Energy Mater 11 (2021). 21011998,. https://doi.org/10.1002/aenm.202101998.

[5] X. Chia, M. Pumera, Characteristics and performance of two-dimensional materials for electrocatalysis, Nat Catal 1 (2018) 909–921. https://doi.org/10.1038/s41929-018-0181-7.

[6] J.D. Benck, T.R. Hellstern, J. Kibsgaard, P. Chakthranont, T.F. Jaramillo, Catalyzing the hydrogen evolution reaction (HER) with molybdenum sulfide nanomaterials, ACS Catal 4 (2014) 3957–3971. https://doi.org/10.1021/cs500923c.

[7] X. Zou, Y. Zhang, Noble metal-free hydrogen evolution catalysts for water splitting, Chem Soc Rev 44 (2015) 5148–5180. https://doi.org/10.1039/c4cs00448e.

[8] C. Zhang, Z. Wang, S. Bhoyate, T. Morey, B. Neria, V. Vasiraju, G. Gupta, S. Palchoudhury, P. Kahol, S. Mishra, F. Perez, R. Gupta, MoS_2 Decorated Carbon Nanofibers as Efficient and Durable Electrocatalyst for Hydrogen Evolution Reaction, C (Basel) 3 (2017) 33. https://doi.org/10.3390/c3040033.

[9] S.C. Lee, J.D. Benck, C. Tsai, J. Park, A.L. Koh, F. Abild-Pedersen, T.F. Jaramillo, R. Sinclair, Chemical and phase evolution of amorphous molybdenum sulfide catalysts for electrochemical hydrogen production, ACS Nano 10 (2016) 624–632. https://doi.org/10.1021/acsnano.5b05652.

[10] B. Hinnemann, P.G. Moses, J. Bonde, K.P. Jørgensen, J.H. Nielsen, S. Horch, I. Chorkendorff, J.K. Nørskov, Biomimetic hydrogen evolution: MoS_2 nanoparticles as catalyst for hydrogen evolution, J Am Chem Soc 127 (2005) 5308–5309. https://doi.org/10.1021/ja0504690.

[11] S. Mansingh, K.K. Das, K. Parida, HERs in an acidic medium over MoS_2 nanosheets: From fundamentals to synthesis and the recent progress, Sustain Energy Fuels 5 (2021) 1952–1987. https://doi.org/10.1039/d0se01683g.

[12] T.F. Jaramillo, K.P. Jørgensen, J. Bonde, J.H. Nielsen, S. Horch, I. Chorkendorff, Identification of active edge sites for electrochemical H2 evolution from MoS_2 nanocatalysts, Science (1979) 317 (2007) 100–102. https://doi.org/10.1126/science.1141483.

[13] J.W.D. Ng, T.R. Hellstern, J. Kibsgaard, A.C. Hinckley, J.D. Benck, T.F. Jaramillo, Polymer Electrolyte Membrane Electrolyzers Utilizing Non-precious Mo-based Hydrogen Evolution Catalysts, ChemSusChem 8 (2015) 3512–3519. https://doi.org/10.1002/cssc.201500334.

[14] P.K.R. Holzapfel, M. Bühler, D. Escalera-López, M. Bierling, F.D. Speck, K.J.J. Mayrhofer, S. Cherevko, C. V. Pham, S. Thiele, Fabrication of a Robust PEM Water Electrolyzer Based on Non-Noble Metal Cathode Catalyst: [Mo3S13]2− Clusters Anchored to N-Doped Carbon Nanotubes, Small 16 (2020) 1–10. https://doi.org/10.1002/smll.202003161.

[15] Y. Li, Y. Yu, Y. Huang, R.A. Nielsen, W.A. Goddard, Y. Li, L. Cao, Engineering the Composition and Crystallinity of Molybdenum Sulfide for High-Performance Electrocatalytic Hydrogen Evolution, ACS Catal 5 (2015) 448–455. https://doi.org/10.1021/cs501635v.

[16] M.A. Lukowski, A.S. Daniel, F. Meng, A. Forticaux, L. Li, S. Jin, Enhanced hydrogen evolution catalysis from chemically exfoliated metallic MoS_2 nanosheets, J Am Chem Soc 135 (2013) 10274–10277. https://doi.org/10.1021/ja404523s.

[17] D. Voiry, M. Salehi, R. Silva, T. Fujita, M. Chen, T. Asefa, V.B. Shenoy, G. Eda, M. Chhowalla, Conducting MoS_2 nanosheets as catalysts for hydrogen evolution reaction, Nano Lett 13 (2013) 6222–6227. https://doi.org/10.1021/nl403661s.

[18] A. Ambrosi, Z. Sofer, M. Pumera, 2H → 1T phase transition and hydrogen evolution activity of MoS_2, $MoSe_2$, WS2 and WSe_2 strongly depends on the MX_2 composition, Chemical Communications 51 (2015) 8450–8453. https://doi.org/10.1039/c5cc00803d.

[19] R.J. Toh, Z. Sofer, J. Luxa, D. Sedmidubský, M. Pumera, 3R phase of MoS_2 and WS2 outperforms the corresponding 2H phase for hydrogen evolution, Chem. Comm. 53 (2017) 3054–3057. https://doi.org/10.1039/c6cc09952a.

[20] A.D. Marinov, L. Bravo Priegue, A.R. Shah, T.S. Miller, C.A. Howard, G. Hinds, P.R. Shearing, P.L. Cullen, D.J.L. Brett, *Ex Situ* Characterization of 1T/2H MoS_2 and Their Carbon Composites for Energy Applications, a Review, ACS Nano 17 (2023) 5163–5186. https://doi.org/10.1021/acsnano.2c08913.

[21] Janjua M.B.I., R.L. Le Roy, Electrocatalyst performance in industrial water electrolyzers, Int J Hydrogen Energy 10 (1985) 11–19.

[22] M. Ledendecker, J.S. Mondschein, O. Kasian, S. Geiger, D. Göhl, M. Schalenbach, A. Zeradjanin, S. Cherevko, R.E. Schaak, K. Mayrhofer, Stability and Activity of Non-Noble-Metal-Based Catalysts Toward the Hydrogen Evolution Reaction, Angewandte Chemie - International Edition 56 (2017) 9767–9771. https://doi.org/10.1002/anie.201704021.

[23] B.E. Conway, H. Angerstein-Kozlowska, M.A. Sattar, B. V. Tilak, Study of a Decomposing Hydride Phase at Nickel Cathodes by Measurement of Open-Circuit Potential Decay, J Electrochem Soc 130 (1983) 1825–1836. https://doi.org/10.1149/1.2120106.

[24] F. Harnisch, G. Sievers, U. Schröder, Tungsten carbide as electrocatalyst for the hydrogen evolution reaction in pH neutral electrolyte solutions, Appl Catal B 89 (2009) 455–458. https://doi.org/10.1016/j.apcatb.2009.01.003.

[25] Z. Wang, Y.R. Zheng, J. Montoya, D. Hochfilzer, A. Cao, J. Kibsgaard, I. Chorkendorff, J.K. Nørskov, Origins of the Instability of Nonprecious Hydrogen Evolution Reaction Catalysts at Open-Circuit Potential, ACS Energy Lett 6 (2021) 2268–2274. https://doi.org/10.1021/acsenergylett.1c00876.

[26] S.C. Escalera-López, Daniel, Christian Iffelsberger, Matej Zlatar, Katarina Novčić, Nik Maselj, Chuyen Van Pham, Primož Jovanovič, Nejc Hodnik, Simon Thiele, Martin Pumera, Allotrope-dependent activity-stability relationships of molybdenum sulfide hydrogen evolution electrocatalysts, Nat Commun 15 (2024) 3601. https://doi.org/10.1038/s41467-024-47524-w.

[27] V.A. Martinez Lopez, H. Ziar, J.W. Haverkort, M. Zeman, O. Isabella, Dynamic operation of water electrolyzers: A review for applications in photovoltaic systems integration, Renewable and Sustainable Energy Reviews 182 (2023). https://doi.org/10.1016/j.rser.2023.113407.

[28] S.A. Grigoriev, D.G. Bessarabov, V.N. Fateev, Degradation mechanisms of MEA characteristics during water electrolysis in solid polymer electrolyte cells, Russian Journal of Electrochemistry 53 (2017) 318–323. https://doi.org/10.1134/S1023193517030065.

[29] P. Aßmann, A.S. Gago, P. Gazdzicki, K.A. Friedrich, M. Wark, Toward developing accelerated stress tests for proton exchange membrane electrolyzers, Curr Opin Electrochem 21 (2020) 225–233. https://doi.org/10.1016/j.coelec.2020.02.024.

[30] A. Weiß, A. Siebel, M. Bernt, T.-H. Shen, V. Tileli, H.A. Gasteiger, Impact of intermittent operation on lifetime and performance of a PEM water electrolyzer, J Electrochem Soc 166 (2019) F487–F497. https://doi.org/10.1149/2.0421908jes.

[31] C. Rakousky, U. Reimer, K. Wippermann, M. Carmo, W. Lueke, D. Stolten, An analysis of degradation phenomena in polymer electrolyte membrane water electrolysis, J Power Sources 326 (2016) 120–128. https://doi.org/10.1016/j.jpowsour.2016.06.082.

[32] J. Chen, J. Mi, K. Li, X. Wang, E. Dominguez Garcia, Y. Cao, L. Jiang, L. Oliviero, F. Maugé, Role of Citric Acid in Preparing Highly Active CoMo/Al2O3 Catalyst: From Aqueous Impregnation Solution to Active Site Formation, Ind Eng Chem Res 56 (2017) 14172–14181. https://doi.org/10.1021/acs.iecr.7b02877.

[33] L.A. Zavala, K. Kumar, V. Martin, F. Maillard, F. Maugé, X. Portier, L. Oliviero, L. Dubau, Direct Evidence of the Role of Co or Pt, Co Single-Atom Promoters on the Performance of MoS_2 Nanoclusters for the Hydrogen Evolution Reaction, ACS Catal 13 (2023) 1221–1229. https://doi.org/10.1021/acscatal.2c05432.

[34] J. Chen, F. Maugé, J. El Fallah, L. Oliviero, IR spectroscopy evidence of MoS_2 morphology change by citric acid addition on MoS_2/Al_2O_3 catalysts - A step forward to differentiate the reactivity of M-edge and S-edge, J Catal 320 (2014) 170–179. https://doi.org/10.1016/j.jcat.2014.10.005.

[35] L. Zavala-Sanchez, X. Portier, F. Maugé, L. Oliviero, High-resolution STEM-HAADF microscopy on a γ-Al_2O_3 supported MoS_2 catalyst - Proof of the changes in dispersion and morphology of the slabs with the addition of citric acid, Nanotechnology 31 (2020) 035706. https://doi.org/10.1088/1361-6528/ab483c.

[36] H. Vrubel, X. Hu, Growth and activation of an amorphous molybdenum sulfide hydrogen evolving catalyst, ACS Catal 3 (2013) 2002–2011. https://doi.org/10.1021/cs400441u.

[37] L. Oliviero, A. Travert, E. Dominguez Garcia, J. Chen, F. Maugé, Catalysis by sulfides: Advanced IR/CO spectroscopy for the identification of the most active sites in hydrodesulfurization reactions, J Catal 403 (2021) 87–97. https://doi.org/10.1016/j.jcat.2021.02.018.

[38] J. Parra-restrepo, Caractérisation des hétérogénéités de fonctionnement et de dégradation au sein d ' un électrolyseur à membrane échangeuse de protons (PEM), 2020. https://theses.hal.science/tel-02942062/.

[39] C. Jacob Bonde, a Poul G. Moses, b Thomas F. Jaramillo, J.K.N. Chorkendorff, ørskovb and Ib, Hydrogen evolution on nano-particulate transition metal sulfides, Faraday Discuss 140 (2008) 219–231. https://doi.org/10.1039/b814058h.

[40] M. Bonanno, K. Müller, B. Bensmann, R. Hanke-Rauschenbach, D. Aili, T. Franken, A. Chromik, R. Peach, A.T.S. Freiberg, S. Thiele, Review and Prospects of PEM Water Electrolysis at Elevated Temperature Operation, Adv Mater Technol 9 (2024) 2300281. https://doi.org/10.1002/admt.202300281.

[41] M. Pourbaix, Atlas d'équilibres électrochimiques à 25°C, Gauthier-Villars & Cie, Paris, 1963.

[42] O. Koyun, S. Gorduk, M.B. Arvas, Y. Sahin, Direct, one-step synthesis of molybdenum blue using an electrochemical method, and characterization studies, Synth Met 233 (2017) 111–118. https://doi.org/10.1016/j.synthmet.2017.09.009.